Effectively parameterizing dissipative particle dynamics using COSMO-SAC: A partition coefficient study

Jonathan Saathoff

Citation: The Journal of Chemical Physics **148**, 154102 (2018); doi: 10.1063/1.5019952
View online: https://doi.org/10.1063/1.5019952
View Table of Contents: http://aip.scitation.org/toc/jcp/148/15
Published by the American Institute of Physics

Effectively parameterizing dissipative particle dynamics using COSMO-SAC: A partition coefficient study

Jonathan Saathoff[a)]
ExxonMobil Research and Engineering Company, Annandale, New Jersey 08801-3059, USA

(Received 18 December 2017; accepted 1 March 2018; published online 20 April 2018)

Dissipative Particle Dynamics (DPD) provides a tool for studying phase behavior and interfacial phenomena for complex mixtures and macromolecules. Methods to quickly and automatically parameterize DPD greatly increase its effectiveness. One such method is to map predicted activity coefficients derived from COSMO-SAC onto DPD parameter sets. However, there are serious limitations to the accuracy of this mapping, including the inability of single DPD beads to reproduce asymmetric infinite dilution activity coefficients, the loss of precision when reusing parameters for different molecular fragments, and the error due to bonding beads together. This report describes these effects in quantitative detail and provides methods to mitigate much of their deleterious effects. This includes a novel approach to remove errors caused by bonding DPD beads together. Using these methods, logarithm hexane/water partition coefficients were calculated for 61 molecules. The root mean-squared error for these calculations was determined to be 0.14—a very low value—with respect to the final mapping procedure. Cognizance of the above limitations can greatly enhance the predictive power of DPD. *Published by AIP Publishing.* https://doi.org/10.1063/1.5019952

I. INTRODUCTION

Hoogerbrugge and Koelman first developed Dissipative Particle Dynamics (DPD) as a particle-based method for simulating liquid flows; it was computationally inexpensive compared with Molecular Dynamics (MD) and offered more flexibility than lattice-gas simulations.[1] Developments by Español, Groot, and Warren permitted DPD simulations to run in canonical ensembles with well-defined relationships between the simulation parameters and the Flory-Huggins χ parameter.[2,3] Since then, researchers have used DPD for a variety of mesoscale kinetic and thermodynamic phenomena, such as determining the phase behavior and rheology of polymers in solution,[4–8] predicting the self-assembly of diblock copolymers,[9–11] studying the properties of bilayer lipid or polymer membranes,[12–16] determining the interfacial tensions between oil and water phases as well as critical micelle concentrations upon the addition of surfactants,[17–23] asphaltene aggregation,[24] and partitioning behavior.[25,26]

Unlike other MD methods, where parameter sets are flexible enough to be applied to many different systems, unique parameter sets are often needed to be devised for DPD simulations representing different conditions and compositions. This is in part due to the lack of realism and simplicity of the interactions between DPD "beads" that represent molecular fragments in a simulation. Therefore, easy-to-use parameterization strategies are necessary for the effective application of DPD. One such strategy is to use the relationship between DPD parameters and the Flory-Huggins χ parameter, as mentioned above.[3] Further developments have increased the precision for relating DPD parameters to measurable properties. For example, Liyana-Arachchi *et al.* devised an accurate equation of state for single DPD beads, and they found an expression relating DPD parameters to the excess chemical potentials of individual beads.[27] In addition, software packages like CULGI include tools to determine DPD parameters for beads with differing applied pressures, excess chemical potentials, and densities over a wide range of possible values.[28] Tools such as these have greatly improved the ability of modelers to parameterize DPD systems.

Along with well-defined relationships between simulation parameters and measurable properties, a source of data is needed to create parameters for DPD simulations. While experimental data are a natural choice, it might not be available and its requirement reduces the predictive power of DPD (some aspects of a system have to be well understood before running a simulation). An alternative would be predictive methods like COSMO-RS (COnductor-like Screening Model for Real Solvents) or COSMO-SAC (COnductor-like Screening Model—Segment Activity Coefficient), which can accurately predict activity coefficients.[29,30] Examples of applying this strategy include the work of Vishnyakov *et al.*, where COSMO-RS was used to parameterize their system of oil, water, and surfactants.[19] More recently, COSMO-RS-parameterized DPD simulations accurately predicted interfacial tensions between *n*-alkane and water interfaces.[31] Fraaije *et al.* also demonstrated a parameterization scheme using COSMO-RS that accurately predicted 1-octanol/water partition coefficients.[25]

While the previously listed studies have effectively parameterized DPD simulations with COSMO-based methods, the quality of the different parameterization schemes is typically related to how well the simulated results match with the experimental data rather than how well the parameterization data maps onto DPD. While the former is certainly important, the

[a)]Electronic mail: jonathan.d.saathoff@exxonmobil.com

latter would quantify limitations that DPD has with representing a system. A modeler could always find a better source of data to parameterize their system, but if DPD is limited in how well it can use that data, there will always be some inherent error in the results.

The aim of this study is to quantify mapping errors between COSMO-SAC data and the resulting DPD parameter set. This includes errors due to mapping COSMO-SAC activity coefficients onto parameters for individual beads, reusing beads for different molecules, and bonding beads together. Here, the calculation of hexane/water partition coefficients using DPD and COSMO-SAC acts as a tool for measuring the magnitude of these various effects. In addition, this report will describe a strategy for reducing some of the error resulting due to bonding DPD beads together to form molecules.

II. SIMULATION METHODS

Equation (1) represents the conservative force, F_{ij}^C, between two DPD beads[16]

$$F_{ij}^C = \begin{cases} A_{ij}\left(1 - \frac{r_{ij}}{r_C}\right) & |r_{ij}| \le r_C \\ 0 & |r_{ij}| > r_C \end{cases}. \tag{1}$$

Here, A_{ij} is the repulsion parameter between beads i and j, which is proportional to how much the two beads repel each other. r_C is the cutoff radius and it is held at a constant value of 1.0 in all cases. r_{ij} is the distance between two particles.

Self-repulsion terms (A_{ii}) between identical beads were used to fix their volumes in simulation, and the cross-repulsion terms ($A_{ij}, j \neq i$) between unlike beads are used to affect partitioning behavior. Unlike other studies where approximate relationships between A_{ij}s and parameters such as infinite dilution activity coefficients and χ are used,[19,31] internal functions within the CULGI software package were applied to relate self- and cross-repulsion terms to excess chemical potentials as well as densities and pressures. Functions such as these can be developed by interpolating the results of many DPD simulations of beads of a single type (for self-repulsion parameters) and single solute beads of one type in a bath of solvent beads of another type (for cross-repulsion parameters). An accurate DPD equation of state, like that produced by Liyana-Arachchi *et al.*, would provide similar utility.[27]

Predicted infinite dilution activity coefficients, γ^∞s, from COSMO-SAC were used to parameterize each DPD simulation. Since CULGI calculates A_{ij}s based on input excess chemical potentials, μ_{ex}s, the relationship between γ^∞ and μ_{ex} needs to be defined (throughout this paper, it is assumed that all μ_{ex}s are calculated at infinite dilution). The activity coefficient, γ, is defined through Eq. (2), with μ being the chemical potential of a molecule in a solution, μ_0 being the chemical potential of a molecule in its pure phase, and x being the mole fraction of that component in a solution (k_B and T are the Boltzmann's constant and temperature, respectively).

$$\mu - \mu_0 = k_B T \ln(\gamma x). \tag{2}$$

Given that μ is the summation of excess chemical potential, μ_{ex}, and the ideal gas chemical potential, Eq. (3) can be derived as follows:

$$k_B T \ln\left(\frac{\gamma_1^\infty}{\gamma_2^\infty}\right) = \mu_{ex,1} - \mu_{ex,2} + k_B T \ln\left(\frac{\rho_1}{\rho_2}\right). \tag{3}$$

Here, the subscripts 1 and 2 refer to two different solutions and ρ refers to the number density of molecules in a solution. Equation (3) was effectively derived by Vishnyakov *et al.*, where the μ_{ex}s were calculated from the Widom insertion method.[19] This derivation is repeated in the supplementary material.

A variant of COSMO-SAC integrated into CULGI was used as a source of data for DPD parameterization. The COSMO-RS and COSMO-SAC methods are very similar. They are described in detail elsewhere[29,30] and will not be repeated here, except for a few relevant points. The γs are predicted in COSMO-SAC by using the volume, surface area, and segment surface charge densities of a molecule generated through a COSMO calculation. These COSMO calculations are made concurrently with a density field theory calculation to determine a molecule's total energy. In these calculations, the molecule of interest sits in a cavity of a conductor-like medium. The distances between the cavity wall and the atoms within the molecule roughly represent the van der Waals radii. The cavity wall is represented as a mesh around the molecule. COSMO calculations provide volumes and surface areas of these cavities, as well as effective segment surface charge densities (charge/segment area), where the segments are defined by the mesh on the cavity wall. $\ln(\gamma)$ can be calculated using these COSMO parameters, and it is the summation of two different components [Eq. (4)].

$$\ln\gamma = \ln\gamma_{res} + \ln\gamma_{comb}. \tag{4}$$

Segment surface charge densities are used to calculate the residual activity coefficient, γ_{res}, and the surface area and volume of the cavity are used to calculate the combinatorial activity coefficient, γ_{comb}, which is calculated through the Staverman-Guggenheim approximation.[32,33] The segments on the cavity wall are typically smaller than the contact area between solute and solvent molecules. Therefore, the raw segment surface charge densities are smoothed with respect to neighboring segment's surface charge density to better represent how nearby molecules "feel" each other.

Since r_C in Eq. (1) is held constant, beads must represent collections of atoms with similar volumes. Therefore, larger molecules must be decomposed into molecular fragments, where each fragment is represented by a single bead. Each of these beads is then bonded together to form the DPD representation of the larger molecule. Fraaije *et al.* discussed this fragmentation scheme in detail, where the decomposition was carried out through a simulated annealing approach.[25] The atoms within the molecule are randomly arranged into different fragments following the simulating annealing approach while maintaining their connectivity until an objective function is minimized. In the case of this study, the objective function was defined such that fragments tended to contain 3 non-hydrogen atoms per fragment (there were no limits placed on the number of hydrogen atoms). In addition to choosing optimal fragments, the connectivity of each fragment with respect to the other fragments in a molecule is recorded as well as the

relative location of each fragment in space. This provides information on how different beads are bonded together in a DPD representation of a molecule as well as what the equilibrium bond lengths and angles should be.

In addition to decomposing the molecular structure, the CULGI software package also splits the total COSMO volume, surface area, and smoothed segment surface charge densities among the fragments based on which atoms are within the fragment. To verify that this scheme did not introduce any errors into the parameterization work flow, μ_{ex}s were compared between full molecules and their fragmented counterparts in hexane and water phases. Since COSMO-SAC calculations do not take into account conformational changes, the sum of the fragmented μ_{ex}s should equal that of the full molecule. Only differences in μ_{ex} are relevant for DPD because the method is limited to simulations in the liquid phase. Therefore, differences in μ_{ex} between the water and the hexane phase were compared rather than their absolute values. Equation (5) [derived from Eq. (3)] was used to calculate the μ_{ex} difference, $\Delta\mu_{ex}$, of the fragments between the hexane and the water phase, where N is the total number of fragments in the molecule and ρ is the bead density in a particular phase.

$$\Delta\mu_{ex} = k_B T \sum_{i=1}^{N} \left[\ln\left(\frac{\gamma^{\infty}_{W,i}}{\gamma^{\infty}_{H,i}} \right) \right] - k_B T\, N \ln\left(\frac{\rho_W}{\rho_H} \right). \quad (5)$$

$\Delta\mu_{ex}$ was calculated for the full molecule and fragments of hexane, nonane, benzene, and toluene. The results of the comparison are shown in Table I. The $\Delta\mu_{ex}$s of the full molecule and the fragments are identical in each case, demonstrating that the fragmentation of the COSMO surface charge density, surface area, and volume is consistent.

To relate DPD units to real units, a bead representing a collection of atoms with well-defined measured properties must be described. Here, this "basis bead" represents 3 molecules of water. Following the work by Groot and Rabone, the volume of three molecules is approximately 90 Å^3 in liquid water at room temperature and atmospheric pressure.[16] The water bead number density per unit volume, ρ_W, was chosen to be 3.0. Using the parameters of this basis bead to convert DPD units to real units, r_C is shown to be 6.463 Å through Eq. (6).

$$r_C = (90\rho_W)^{1/3}. \quad (6)$$

The total COSMO volume of each fragment, V_{frag}, is then used to calculate DPD fragment densities, ρ_{frag}, based on the COSMO volume of the water DPD bead, V_W [Eq. (7)]. COSMO-based calculations assume an incompressible liquid medium. Therefore, only constant pressure simulations should be attempted unless it can be shown that changes in density for each of the components correctly correspond to changes in pressure.

$$\rho_{frag} = \rho_W \frac{V_W}{V_{frag}}. \quad (7)$$

The water self-repulsion term was set to 25.0. Setting this parameter to a low value allowed the maximum number of other calculated parameters to be within CULGI's permitted range. This does not achieve the correct isothermal compressibility. However, other groups have shown that this is not important for the simulations in this paper.[25,26] The self-repulsion terms of all the other beads were set such that their relative densities compared with that of water could be reproduced using Eq. (7). The procedure used to calculate cross-repulsion parameters will be discussed in Sec. III.

Once DPD parameters were devised, the hexane/water partition coefficient, K_{HW}, was calculated in terms of mole fractions. While a simulation could be set up to calculate K_{HW} by creating a hexane/water interface and tabulating the average mole fraction of the molecule in the hexane and water phases (x_H and x_W, respectively), it is more efficient to calculate the γ^{∞}s in the two phases (γ^{∞}_H and γ^{∞}_W). Since the μs of the solute in the two phases must be equal, Eq. (2) can be used to derive Eq. (8), showing how these terms can be related.

$$K_{HW} = \frac{x_H}{x_W} = \frac{\gamma^{\infty}_W}{\gamma^{\infty}_H}. \quad (8)$$

Two sets of simulations were run in LAMMPS for each molecule in order to calculate the activity coefficients—one set in a bath of hexane and the other set in a bath of water.[34] In each set, the μ_{ex} of the molecule was calculated using Thermodynamic Integration (TI) applied in a similar fashion as done by Fraaije *et al.*[21] These μ_{ex}s combined with Eq. (3) were used to calculate γ^{∞}s. TI was implemented by incorporating a coupling parameter, λ, into the conservative force between the solute and the solvent when $r_{ij} \le 1.0$ [Eq. (9)].

$$F^C_{ij} = \lambda A_{ij} \left(1 - \frac{r_{ij}}{r_C} \right). \quad (9)$$

To calculate each μ_{ex}, 16 simulations were run, each having a value of λ between 0 and 1. In each simulation, the average derivative of the system's Hamiltonian, H, with respect to λ was calculated. This can be related to the free energy, G, through Eq. (10).

$$\frac{\partial G}{\partial \lambda} = \left\langle \frac{\partial H}{\partial \lambda} \right\rangle. \quad (10)$$

Numerically integrating this derivative across λ provides the free energy required to add the molecule to the solution, or μ_{ex}.

In this study, unless otherwise noted, a time step of 0.01 was used to run each DPD simulation. Each simulation was held in an NPT ensemble through the use of a Berendsen barostat. With this method, it was found that a pressure of 23.735 $k_B T/r_C^3$ was required to keep water beads at a density of 3.0; therefore, the pressure was fixed to this value in each simulation. Each simulation was equilibrated over 50 000 time

TABLE I. Comparison of total $\Delta\mu_{ex}$s between hexane and water phases of several different molecules in full and fragmented form.

Molecule type	Full molecule $\Delta\mu_{ex}$ ($k_B T$)	Fragmented sum $\Delta\mu_{ex}$ ($k_B T$)
Hexane (2 beads)	9.34	9.34
Nonane (3 beads)	12.97	12.97
Benzene (2 beads)	4.64	4.64
Toluene (2 beads)	5.89	5.89

steps, and then the data were collected over 200 000 time steps. In addition, the DPD conservative force between beads within the same molecule was set to zero. All intramolecular beads were held at a fixed relative geometry so that all equilibrium bond lengths and angles determined from CULGI's fragmentation routine were maintained. Despite the somewhat unrealistic rigidity, the parameterization scheme described is similarly effective for flexible molecules (see Sec. S6 of the supplementary material).

In addition to the conservative force, F_{ij}^C, shown in Eq. (1), there are random and dissipative forces, F_{ij}^C and F_{ij}^D, which also occur between interacting particles.[3] The magnitude of these forces is defined in Eqs. (11a)–(11c),

$$F_{ij}^D = -\alpha \left(1 - \frac{r_{ij}}{r_C}\right)\left(\hat{r_{ij}} \cdot \hat{v_{i,j}}\right), \tag{11a}$$

$$F_{ij}^R = \sigma \left(1 - \frac{r_{ij}}{r_C}\right)^2 \zeta \Delta t^{-1/2}, \tag{11b}$$

$$\sigma^2 = 2\alpha k_B T. \tag{11c}$$

The noise amplitude, σ, is set to 3.0. k_BT is set to 1.0 (the effects of temperature on the parameterization are made through the COSMO calculations) following the work by Groot and Warren.[3] v_{ij} is the relative velocity between the two particles, and the hats above v_{ij} and r_{ij} indicate unit vectors. ζ is a random variable with a unit variance and a zero average, and α is a friction factor that is dependent on the values of k_BT and σ. All forces are zero if r_{ij} is greater than r_C.

III. RESULTS AND DISCUSSION

A. Parameterizing DPD beads

To test the various parameterization strategies for DPD, the hexane/water partition coefficients for 61 molecules were calculated. These molecules were taken from the original COSMO-SAC paper by Lin and Sandler.[30] In that study, 64 molecules were used, but the partition coefficients for three of the molecules were not calculated in this report because some of their interactions require DPD parameters that are outside the allowable range in CULGI. These molecules are listed in Table S1 of the supplementary material.

As stated earlier, the cross-repulsion terms control the partitioning behavior between beads. Figure 1(a) shows the $\ln(\gamma)$s of two different bead types labeled 1 and 2 in solutions of both types of beads (here, the time step size and number were set to 0.02 and 400 000, respectively, to increase sampling and produce smoother curves). In either case, their self-repulsion parameters, A_{11} and A_{22}, are equal to 25.0. With an A_{12} above 25.0, $\ln(\gamma)$ is greater than or equal to zero, showing that the beads prefer not to mix. Alternatively, with an A_{12} below 25.0, $\ln(\gamma)$ is less than zero. Similar behavior occurs when changing the self-repulsion terms as shown in Fig. 1(b). Here, A_{11} and A_{12} are fixed at 25.0, while A_{22} is altered. An important feature is that, for specified repulsion parameters, the plots of $\ln(\gamma)$ for bead type 1 and 2 are mirror images of each other in Fig. 1(a) and almost mirror images of each other in Fig. 1(b).

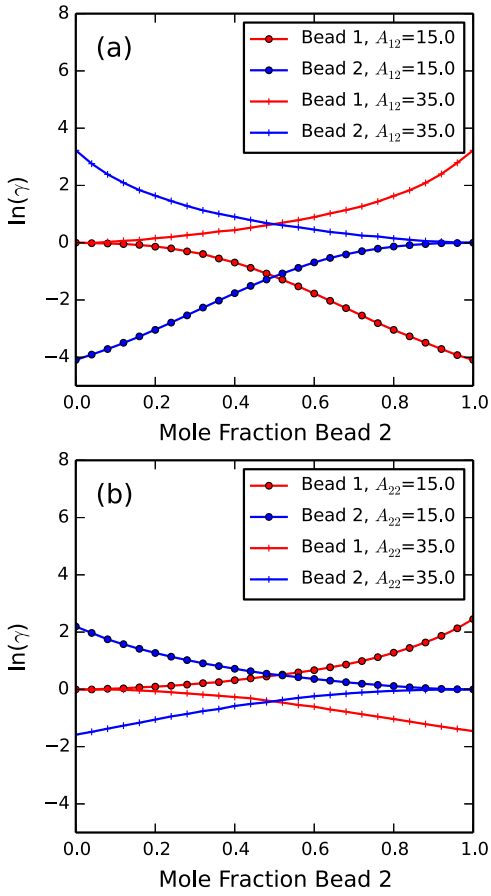

FIG. 1. Activity coefficients for bead 1 and bead 2 as a function of solvent composition. (a) shows the effect of changing cross-repulsion terms (A_{12}) and (b) shows the effect of changing one of the two self-repulsion terms (A_{22}). All repulsion parameters not defined in the legend are set to 25.0.

COSMO-SAC-calculated $\ln(\gamma)$s are more complicated. Figure 2 shows $\ln(\gamma)$s for acetone and a grouping of 3 water molecules (both would be represented by single beads in DPD). There is a 5.5 offset between acetone and water $\ln(\gamma^\infty)$s. DPD cannot reproduce this level of asymmetry between the γ^∞s.

To understand the scope of this problem, the 64 molecules in the Lin and Sandler study were fragmented into 112 unique beads.[30] Between every pair of beads (i and j), the offset,

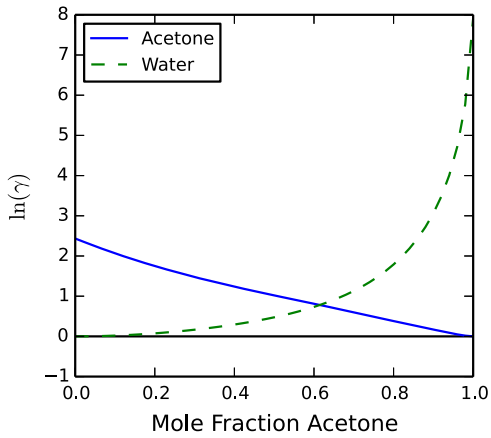

FIG. 2. $\ln\gamma$s of acetone and water in acetone/water mixtures with various acetone mole fractions.

$\Delta\ln\left(\gamma_{ij}^{\infty}\right)$ was calculated just like that for the acetone and water given above, where $\Delta\ln\left(\gamma_{ij}^{\infty}\right)$ is the difference between $\ln(\gamma^{\infty})$s of the two beads being compared. Finally, Eq. (12) was used to calculate the root mean-squared offset, Δ_{RMS}, for each bead i.

$$\Delta_{RMS,i} = \sqrt{\frac{\sum_{j\neq i}^{N}\left(\Delta\ln(\gamma_{ij}^{\infty})\right)^2}{N-1}}. \tag{12}$$

Here, j is a different bead type and N is the total number of beads. While the average value for Δ_{RMS} was 2.7, water induced the greatest offset with a Δ_{RMS} at 23.1. All the other beads had a Δ_{RMS} less than 5.2 (the distribution of Δ_{RMS} is shown in Fig. S1 of the supplementary material). In fact, much of the Δ_{RMS} for the other fragments is due to their interactions with water. Therefore, the modeler should be careful when water is one of the components being simulated with DPD.

In this study, γ^{∞}s were chosen to parameterize each simulation to be consistent with how the simulation was constructed. For example, when μ_{ex} of a solute in hexane was being calculated, γ^{∞}s of the solute fragments at infinite dilution in hexane fragments were used. A similar procedure was used for calculating μ_{ex}s in water. Since the conservative force between beads within the same molecule was set to zero, most other cross-repulsion terms did not have to be defined. In Sec. III D, a solvent comprising of 1-octanol and water is discussed. Since neither species was at infinite dilution, the cross-repulsion terms between the water and 1-octanol were chosen so that the simulated $\ln(\gamma^{\infty})$ is the average between the $\ln(\gamma^{\infty})$s for the beads in 1-octanol and water.

Occasionally, researchers use estimates of COSMO parameters for their molecular fragments. For example, Vishnyakov *et al.* used the COSMO parameters for full molecules to represent the properties of molecular fragments—like using an *n*-octane molecule to represent an alkane chain on a surfactant molecule.[19] More recently, Alasiri and Chapman represented fragments of various sizes by full *n*-alkane molecules in their study of interfacial tension.[31] In addition to applying data from full molecules to molecular fragments, one might want to reuse fragments to limit the total number of bead types in their simulations.

Figure 3 shows an example where a bead representing a propyl group could potentially be reused. Despite the fact that the structure of the propyl group is identical in the butyric acid and hexane molecules, the COSMO parameters are different due to differences in the connecting fragments. Therefore, beads representing the propyl groups in the two molecules would be expected to have two different sets of repulsion parameters. Unless otherwise stated, beads were not reused for different molecules in this study.

Given the potential issues and resulting parameterization procedure just discussed, logarithm hexane/water partition coefficients, $\log(K_{HW})$s, were calculated. In addition to the procedure described above, all bonds and angles in the simulation were held rigid so that the conformation of the DPD molecules remained constant like that in the COSMO-SAC calculations. The parity plot in Fig. 4 compares the resulting $\log(K_{HW})$s calculated with DPD against those calculated directly with COSMO-SAC. Hexane was chosen as the organic phase because the molecule is represented by only two beads with identical repulsion parameters. Therefore, the structure of the molecule should play a negligible role in the simulations, and it would be expected that the COSMO-SAC and DPD results should closely match if the parameterization scheme was effective.

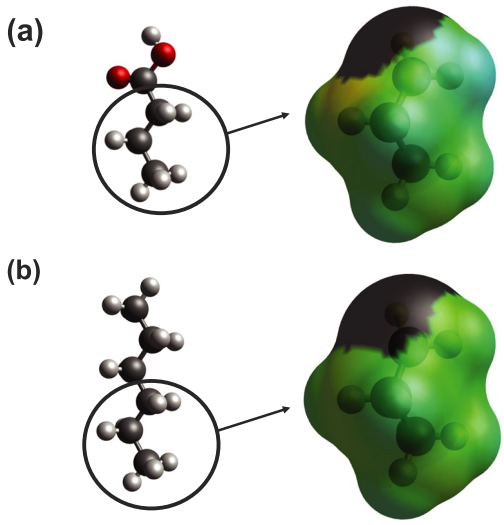

FIG. 3. *n*-propyl fragments from (a) butyric acid and (b) hexane. The surface area and volume for (a) is 81.0 Å^2 and 75.3 Å^3, respectively, while the surface area and volume for (b) is 77.8 Å^2 and 72.4 Å^3, respectively. In addition to these differences, the surface charge density also varies between the fragments. Black portions of the surface symbolize a lack of charge density being present (this portion of the fragment overlaps with the connecting fragment), and the colored surface represents surface charge density, with blue and red hues being the extrema of positive and negative charges, respectively. Note how the amount of charge density (non-black space) and the appearance of red and blue hues differ between fragments (a) and (b).

In Fig. 4, the Root Mean-Squared Error (RMSE) of $\log(K_{HW})$ is 0.74, while the Maximum Absolute Deviation (MAD) is 2.07. While solute molecules represented by a single bead fall on the diagonal, the K_{HW}s of the multi-beaded molecules are typically off the diagonal and the deviation increases the farther $\log(K_{HW})$ is from 0.0. It is clear that the act of bonding beads together affects their partitioning behavior.

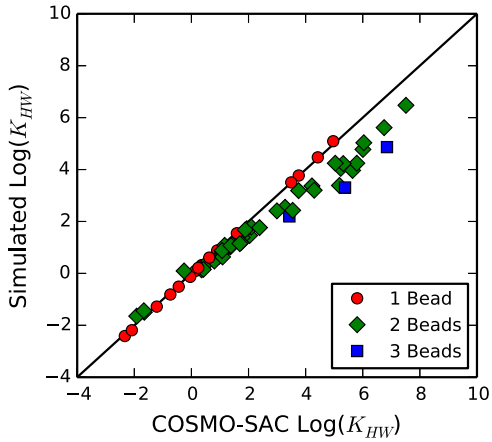

FIG. 4. Parity plot for $\log(K_{HW})$s calculated for different solute molecules directly with COSMO-SAC and DPD. The different symbols represent the number of beads that make up a particular solute molecule.

B. The effects of bonding

To show how bonding DPD beads together affects their partitioning behavior, two sets of simulations were run to compare the μ_{ex}s of individual beads and bonded beads. In all the cases, the self-repulsion parameter of the solvent was 25.0 and the cross-repulsion parameter between the solute and the solvent was 15.0, 25.0, or 35.0. Each curve in Fig. 5(a) shows the results from the first set of simulations, where the differences in total μ_{ex} between two solute beads bonded together and two individual solute beads of the same type are plotted. If the bond length is greater than 1.0, which is the cutoff radius, r_C, there is almost no difference between the μ_{ex}s. However, if the bond length is less than 1.0, the μ_{ex} for the bonded beads can be lower than that of single beads by −7.1 k_BT if the cross-repulsion term is 35.0. When the bond length is less than 1.0, bonded solute beads shield each other from the solvent by pushing solvent beads away from their partner. This reduces the interactions between each solute bead with the solvent, which reduces the μ_{ex} of the bonded solute beads relative to the solute beads if they were not bonded. With a smaller bond length, the solute beads shield each other to a greater extent, lowering μ_{ex} even further. This "bonded solute effect" is the first of three effects bonding has on the system (Fig. 6 shows a diagram of these effects).

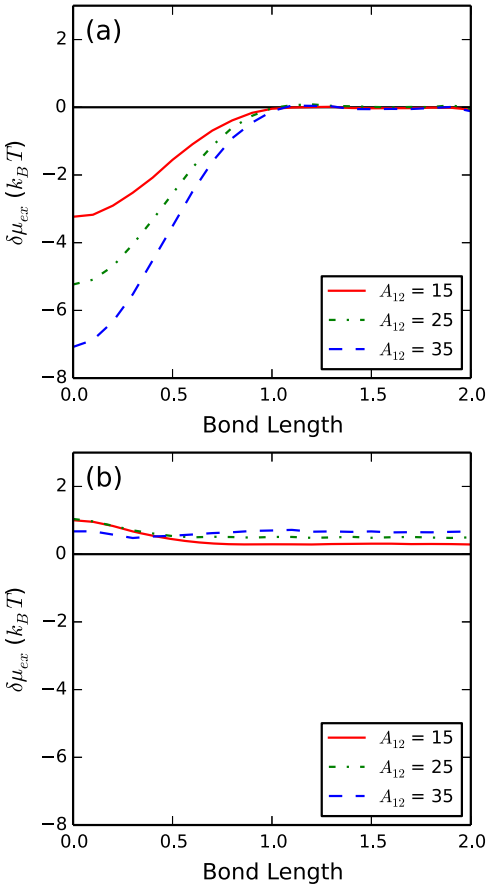

FIG. 5. (a) shows the difference in μ_{ex} ($\delta\mu_{ex}$) between double-beaded solutes with different bond lengths and two non-bonded solute beads in a solution of single beads and (b) shows the $\delta\mu_{ex}$ between single solute beads in a solvent of double-beaded molecules and the same single solute beads in a solvent of single beads. Each curve represents different cross-repulsion parameters between the solvent and the solute. All repulsion parameters not defined in the legend are set to 25.0.

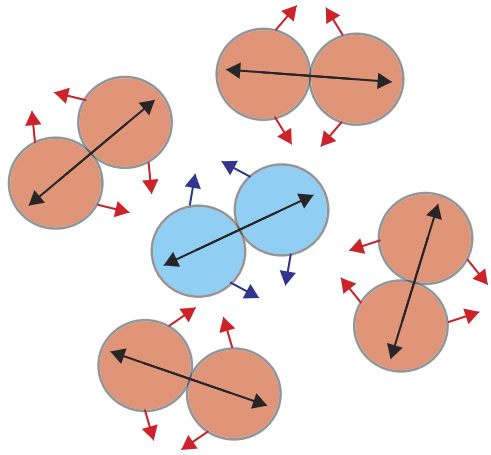

FIG. 6. A diagram representing the effects bonding has on μ_{ex}, with the red beads representing solvent molecules and the blue beads representing the solute molecule. The blue arrows represent the "bonded solute effect," where bonded solute beads push away the solvent beads. The red arrows represent the "bonded solvent effect," where bonded solvent beads push away the solute and other solvent beads. The black arrows represent the "density effect," where forces on the bond causes the density to increase.

Figure 5(b) shows the second case, where the differences in μ_{ex} are calculated between single solute beads in a solvent of double-beaded molecules and single solute beads in a solvent of single beads. Regardless of bond length, the μ_{ex} of the solute bead in bonded solvent is always greater than the μ_{ex} in single beaded solvent. In the simulation box, each bond contributes $-2/(3V)$ to the total pressure of the system, independent of bond length (V being the volume of the system). In an NPT ensemble, this increases the system's density. For example, the density is approximately 3.0 for the solvent of single beads, while the density is 3.1 for the solvent of 2-beaded molecules. With a cross-repulsion parameter of 25.0 (which is the same as the self-repulsion parameters), the μ_{ex}s resulting from this "density effect" are consistent with Flory-Huggins theory, with the difference equaling 0.5 k_BT.[35] However, there is a slight spread between lower and higher cross-repulsion parameters.

The third effect occurs when the bond lengths are less than 1.0. The curves bend and cross each other at a distance of 0.4. The bonds in the solvent cause the solvent beads to have a different local structure around the solute molecule than in the single-beaded solvent. This "bonded solvent effect" is much smaller than the bonded solute and density effects.

The various bonding effects are, to an extent, self-canceling. The μ_{ex}s of a multi-beaded solute molecule will be lower in any phase where the cross-repulsion parameters are greater than 0.0 than if the molecule had no bonds. Since the partition coefficients are related to μ_{ex} differences through the activity coefficients, much of the error will disappear. However, this is not the case where the solute interacts with the two solvents very differently, which is reflected in very low or high values of the partition coefficient. This is why the DPD log (K_{HW})s increasingly deviate from the COSMO-SAC results as their magnitudes increase or decrease from a value of 0.0 in Fig. 4.

C. Bond error corrections

There were significant parameterization errors present in the previous calculation of K_{HW} due to the presence of bonds. The bond lengths of the 61 solute molecules range from 0.29 to 0.81; therefore, all three effects described in Sec. III B would be applicable in this system. One way to reduce these errors is to change the coarse graining scheme so that the bond lengths are as long as possible in DPD units. However, there will typically always be some error due to bonding the DPD beads together unless many heavy atoms are assigned to each DPD bead. Alternatively, adjusting the repulsion parameters can reduce some of the error due to bonding, as discussed below.

The μ_{ex} for single beads is a function of the cross-repulsion parameter between solute bead i and solvent bead S (A_{iS}), the self-repulsion parameter of the solvent, and the density of the solvent. In the present discussion, only μ_{ex}'s dependence on A_{iS} is discussed ($\mu_{ex} \sim \mu_{ex}(A_{iS})$). For example, if the solvent's self-repulsion parameter and density are 25.0 and 3.0, respectively, an A_{iS} of 25.0 will return a μ_{ex} of $\mu_{ex}(A_{iS}) = \mu_{ex}(25.0) = 12.1 k_B T$. This can be calculated through CULGI's internal functions, DPD simulations, or other correlations. μ_{ex}^{err} is the difference in chemical potential between bonded solute beads and non-bonded solute beads, and it needs to be estimated in order to determine how to correct for the bond effects. When the bond length, r_B, for a double-beaded solute is greater than or equal to 1.0, μ_{ex}^{err} should be close to 0.0 $k_B T$. When r_B is 0.0, the two solute beads, 1 and 2, are directly on top of each other. In effect, the dimer behaves as a single effective bead with a cross-repulsion parameter of $A_{1S} + A_{2S}$. In this case, Eq. (13) provides the value of μ_{ex}^{err}.

$$\mu_{ex}^{err} = \mu_{ex}(A_{1S} + A_{2S}) - \mu_{ex}(A_{1S}) - \mu_{ex}(A_{2S}). \tag{13}$$

If A_{1S} and A_{2S} are both set at 25.0, $\mu_{ex}(A_{1S} + A_{2S}) = \mu_{ex}(50.0) = 19.1 k_B T$. Since the μ_{ex} of a single bead is 12.1 $k_B T$, μ_{ex}^{err} will be −5.1 $k_B T$. This is consistent with the results depicted in Fig. 5(a).

This concept is also true if more than two beads totally overlap each other. Since μ_{ex}^{err} decreases as r_B increases, A_{2S} can be replaced by an effective background repulsion parameter, $A_{2,back}$, which is defined in Eq. (14).

$$A_{2,back} = f_S(r_B, A_{2S}) A_{2S}. \tag{14}$$

Here, f_S is a scaling factor between 0.0 and 1.0 and is a function of r_B and A_{2S}. The error due to multiple beads, j, bonded to bead 1 can be estimated by summing each contributing $A_{j,back}$ together [Eq. (15)].

$$\mu_{ex}^{err} = \mu_{ex}(A_{1S} + \sum_j A_{j,back}) - \mu_{ex}(A_{1S}) - \sum_j \mu_{ex}(A_{j,back}). \tag{15}$$

Estimating μ_{ex}^{err} requires f_S to be defined. This was accomplished by first running a series of simulations with bonded pairs of solute beads (bead 1 and bead 2) in a solvent of single S beads. A_{1S} and the solvent self-repulsion terms were held at 25.0, while A_{2S}s from 15.0 to 105.0 in increments of 10.0 were applied. In addition, r_Bs were selected from 0.0 to 2.0 in increments of 0.1, leading to a set of 210 combinations of parameters. For each combination of parameters, TI calculations were executed with the coupling parameter, λ, applied as a coefficient to A_{1S}, with the rest of the interactions fully enabled. The calculated excess chemical potential, μ_{ex}^{calc}, is related to f_S by Eq. (16). μ_{ex}^{calc} was calculated directly through the DPD TI simulations and was only used as a means to find f_S.

$$\mu_{ex}^{calc} = \mu_{ex}(A_{1S} + f_S(r_B, A_{2S}) A_{2S}) - \mu_{ex}(f_S(r_B, A_{2S}) A_{2S}). \tag{16}$$

Using Eq. (16), f_S could be determined for each combination of parameters with $r_B \leq 1.0$ (f_S was insignificant for larger r_B). Estimated values for f_S with $A_{2S} = 15.0$ and 105.0 are shown in Fig. 7. It is noted that f_S for $A_{2S} = 15.0$ does not go to zero as r_B approached 1.0. This is due to limitations in CULGI for calculating μ_{ex} at small $A_{2,back}$. However, the error is small and it only occurs for r_B larger than most of the solute molecules' bonds used in this study.

Curves were fit using the generalized reduced gradient algorithm in order to generate a formula for f_S, as shown in the resulting Eqs. (17a)–(17c). This functional form for f_S was chosen for its simplicity and ability to fit the data well within the range it was used. It should be noted that in Fig. 7, the curve does not fit well for $A_{2S} = 105.0$ and $r_B < 0.2$. However, it would be unusual to have bond lengths this small and no bond was this short in this partitioning study. With f_S being defined, μ_{ex}^{err} can be estimated. The raw data for calculating f_S can be found in the supplementary material.

$$f_S = 1.0 - 0.985 r_B + g(A_{2S}) r_B (1.0 - r_B) + h(A_{2S}) r_B^2 (1.0 - r_B), \tag{17a}$$

$$g = -0.0185 A_{2S} + 1.130, \tag{17b}$$

$$h = 0.0212 A_{2S} - 2.44. \tag{17c}$$

An important fact to note is that f_S is relatively independent of density, the self-repulsion parameter, and A_{1S}. Therefore, this f_S can be applied in situations where these other parameters have different values. f_S is set to 0.0 if $r_B > 1.0$.

The following bond correction scheme represents a simple way to reduce the bonded solute effect. This was done

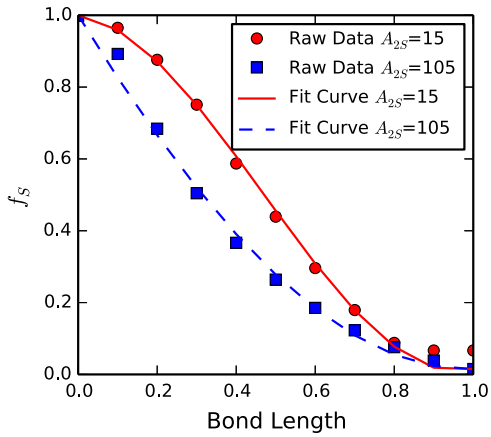

FIG. 7. This plot shows the scaling factor at several different bond lengths with $A_{2S} = 15.0$ and 105.0. The raw data points were collected from simulation results.

by using CULGI's functionality to calculate μ_{ex}s in a short computer script. First, μ_{ex} must be calculated for each individual bead making up a molecule as though it were not connected to any other bead in a single-beaded solvent. The total of these effective μ_{ex}s, or μ_{ex}^{eff}s, is the desired total μ_{ex} of the molecule. Second, the cross-repulsion parameters of each bonded bead, A_{iS}, are modified in order to make up for the bond error, μ_{ex}^{err}. Since each bond is connected to two beads, each A_{iS} must be corrected to make up one half of the total μ_{ex}^{err} it is associated with. This leads to a system of non-linear equations, with the number of equations equalling the number of atoms in the molecule [Eq. (18)].

$$\mu_{ex,i}^{eff} = \mu_{ex}(A_{iS}) + \frac{1}{2}\mu_{ex}^{err}(A_{iS}, \sum_{j\neq i} A_{j,back}). \tag{18}$$

Here, the expression for μ_{ex}^{err} is defined in Eq. (15). This system can be solved using Broyden's method.[36] In addition, if one is using a linear expression of μ_{ex} to determine cross-repulsion terms, and f_S is assumed to be a weak function of the cross-repulsion terms, Eq. (18) could be solved as a system of linear equations.

This bond correction scheme was applied to the simulations shown in Fig. 5. The bond corrections were first applied to interactions where the solute and solvent beads were of the same type. This was needed in order to obtain updated self-repulsion parameters for subsequent calculations. Next, bond corrections were applied between all the possible remaining pairs of beads in the bonded molecules. Results for $r_B = 0.0$ are not presented because the resulting μ_{ex}s are outside the range for which CULGI can calculate repulsion parameters.

Figure 8(a) shows the results of this bond correction scheme for a bonded molecule in a solvent of single-beaded molecules. Comparing with Fig. 5(a), it is clear that the bonded solute effect is almost totally removed. There is a small dip in the curves around 0.9 due to the limitations in CULGI described earlier. With other expressions for μ_{ex} which function over wider ranges of the cross-repulsion parameter, a better fit in Fig. 8(a) could be achieved. Also, there is a small dip approaching $r_B = 0.0$ due to the misfit already discussed.

Figure 8(b) shows that there are some changes due to the bond corrections at r_B less than 1.0 by comparing it with Fig. 5(b). First, the ordering of the curves has changed with no cross-over (the difference in μ_{ex} for $A_{12} = 35.0$ is now greater than $A_{12} = 15.0 \times 2.0\ k_BT$ when $r_B = 0.1$). The changes seen in Fig. 5(b) seem somewhat deleterious. However, the error is significantly smaller than the bonded solute effects without the bond correction. Therefore, the trade-off appears warranted.

D. Results summary

The hexane/water partition coefficients shown in Fig. 4 were recalculated with bond corrections. First, the bond correction scheme was applied to the hexane molecule in a solvent made up of individual hexane beads. This did not have to be repeated for water because water is represented by a single-beaded molecule. Next, bond corrections were applied to the solute molecules in solvents made up of individual hexane beads and water beads. Figure 4 compares the bond-corrected DPD results with COSMO-SAC results. The RMSE and MAD

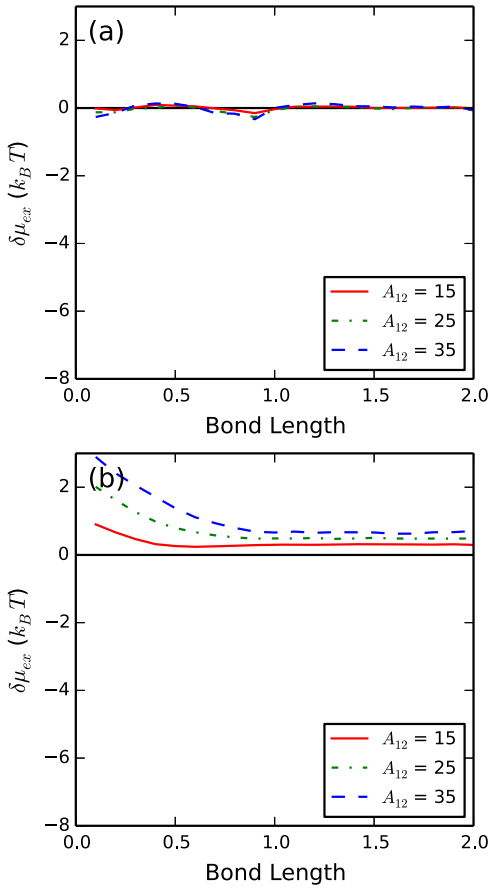

FIG. 8. This figure is identical to Fig. 5, except that bond corrections are applied. (a) shows the difference in μ_{ex} ($\delta\mu_{ex}$) between double-beaded solutes with different bond lengths and two non-bonded solute beads in a solution of single beads and (b) shows the $\delta\mu_{ex}$ between single solute beads in a solvent of double-beaded molecules and the same single solute beads in a solvent of single beads. Each curve represents different cross-repulsion parameters between the solvent and the solute.

of the logarithm partition coefficients were calculated to be 0.14 and 0.40, respectively. This is a significant improvement over the results shown in Fig. 4, with the results in Fig. 9 showing very close parity with the COSMO-SAC results. These results demonstrate that this parameterization scheme effectively maps COSMO-SAC data onto DPD parameter sets.

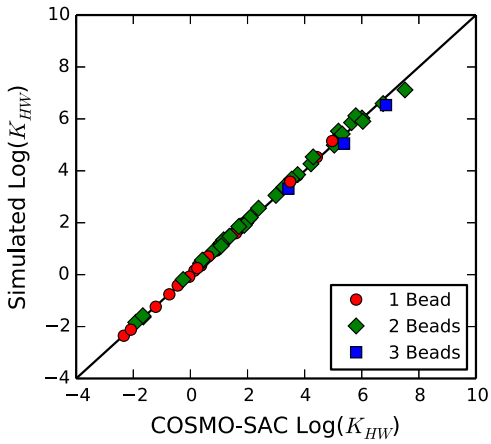

FIG. 9. A parity plot for bond-corrected log (K_{HW})s calculated for different solute molecules with DPD and COSMO-SAC.

Partition coefficients were also calculated for a more complicated system following the same parameterization scheme: 1-octanol and water. Here, 3 course-grained beads represent 1-octanol. Unlike hexane, where the two beads represent identical fragments, 1-octanol has one bead representing a hydroxyl group and two beads representing alkyl groups. This suggests that the 1-octanol solvent might exhibit structure-dependent properties not present in COSMO-SAC. The 1-octanol phase also includes 0.27 mol fraction water.[25] In DPD, this is equivalent to having a mole fraction of 0.11 water beads in the 1-octanol phase.

Figure 10 compares the 1-octanol/water partition coefficients, K_{OW}, calculated with DPD and COSMO-SAC. The RMSE and MAD of the resulting $\log(K_{OW})$s were 0.45 and 0.92, respectively. The deviation from parity was correlated to how much the solute was associated with the hydroxyl or the alkyl groups in 1-octanol—a property that would not be taken into account in the COSMO-SAC calculations.

Experimental partition coefficients are measured on the basis of molar concentrations rather than mole fractions. Therefore, molar concentrations need to be related to activity coefficients to compare experimental results with predictions from COSMO-SAC or DPD. Equation (19) shows this relation for 1-octanol and water, with K^C_{OW} being the partition coefficient in terms of molar concentration.

$$K^C_{OW} = \frac{C_O}{C_W} = \frac{C^{tot}_O x_O}{C^{tot}_W x_W} = \frac{C^{tot}_O \gamma^\infty_W}{C^{tot}_W \gamma^\infty_O} = 0.148\frac{\gamma^\infty_W}{\gamma^\infty_O}. \tag{19}$$

Here, the subscripts O and W represent the 1-octanol-rich and water-rich phases, respectively. C_O and C_W are the molar concentrations of the solute in the two phases, C^{tot}_O and C^{tot}_W are the total molar concentrations of the two phases (8.229 mol/L for the octanol-rich phase and 55.679 mol/L for the water-rich phase), and the xs are the mole fractions of the solute in either phase. This formulation was obtained from Lin and Sandler.[37]

With respect to experiment, CULGI's COSMO-SAC predicts $\log\left(K^C_{OW}\right)$s that have a RMSE of 0.54 and a MAD of 1.52 over the same set of solute molecules used for the DPD simulations, except those without associated experimental data.[30] A parity plot of these data is in Fig. S2 of the supplementary material.

In order to compare the DPD results with the experiment, a correction was needed to be applied to the DPD-calculated activity coefficients to make up for the fact that the DPD water bead was made up of three water molecules instead of one. The COSMO-SAC calculations on the molecular fragments needed to parameterize DPD was the step in the parameterization procedure that introduced this discrepancy. Equation (4) shows that the COSMO-SAC-predicted activities are made up of a residual term and a combinatorial term. The residual term, which uses smoothed surface charge densities, is independent of the size and shape of solvent molecules, so it is unaffected by the number of water molecules in a water bead so long as water is the solvent. However, this is not the case with the combinatorial term. This information can be used to correct the DPD results by applying Eq. (20).

$$K_{OW} = \frac{\gamma^\infty_{W,DPD}}{\gamma^\infty_{O,DPD}} \frac{\gamma^\infty_{1W,comb}}{\gamma^\infty_{3W,comb}}. \tag{20}$$

Here, $\gamma^\infty_{W,DPD}$ and $\gamma^\infty_{O,DPD}$ are the DPD-calculated infinite dilution activity coefficients of the solute in the water-rich and 1-octanol-rich phases, respectively. $\gamma^\infty_{3W,comb}$ is the combinatorial infinite dilution activity coefficient of the solute in a solvent of beads made up of three water molecules, while $\gamma^\infty_{1W,comb}$ is the combinatorial infinite dilution activity coefficient of the solute in a solvent of single water molecules. This can be derived by assuming that the DPD-calculated activity coefficients are equal to the COSMO-SAC-predicted values and by applying Eq. (4).

With this correction, the RMSE and MAD for the $\log\left(K^C_{OW}\right)$s are 0.53 and 1.74, respectively, and a parity plot is shown in Fig. 11. These errors are almost identical to the COSMO-SAC results, indicating that the quality of the COSMO-SAC-calculated activity coefficients is currently the most significant limitation to prediction accuracy. However, if the correction in Eq. (20) is not applied, the error increases to an RMSE and MAD of 1.13 and 3.07, respectively. This shows that having beads of multiple water molecules has a small but

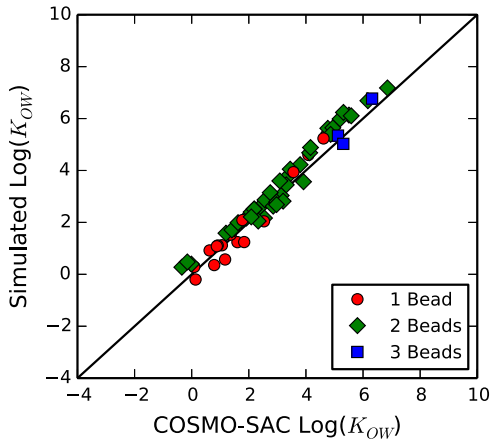

FIG. 10. A parity plot for bond-corrected $\log(K_{OW})$s calculated for different solute molecules directly with DPD and COSMO-SAC.

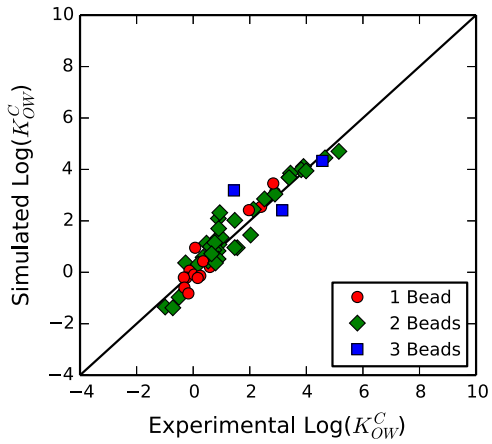

FIG. 11. A parity plot for bond-corrected $\log\left(K^C_{OW}\right)$s calculated for different solute molecules directly with DPD compared with the experiment.

TABLE II. A list showing the deviation of DPD-calculated partition coefficients with respect to COSMO-SAC results following different parameterization procedures.

Organic phase	Special conditions	RMSE [log(K)]	MAD [log(K)]
Hexane	None	0.14	0.40
Hexane	No Bond Correction	0.74	2.07
Hexane	Average Activities	3.67	7.70
Hexane	Non-Unique Beads	0.67	1.43
1-octanol	None	0.45	0.92

significant deleterious impact on the overall quality of the predictions made by DPD. The parity plot for these data is given in Fig. S3 of the supplementary material.

To conclude this discussion, Table II shows a summary of the disparities between COSMO-SAC and DPD results in terms of log (K)s. The special conditions column refers to alterations in the full parameterization scheme described above, with "None" representing the results in Fig. 9 and "No Bond Correction" representing the results from Fig. 4.

For the partition coefficients calculated with "Average Activities," the cross-repulsion parameters between solvent and solute beads were chosen from the average of the two γ^{∞}s of the bead pair rather than choosing the γ^{∞} calculated when each bead is correctly identified as solvent or solute. This alteration created a great deviation away from the COSMO-SAC results (the predictions from this method would not be useful), indicating that the modeler should be cautious when choosing the γ^{∞}s to parameterize the cross-repulsion terms with, especially when there are multiple solvent phases in a system.

"Non-Unique Beads" indicates that different solute molecules shared bead types if they included identical fragments. The deviation due to this procedural change is not as great as the other two; however, it is still significant. The modeler should be careful when using a fragment's COSMO parameters to parameterize beads representing similar fragments on different molecules. This extends to situations where one might use COSMO parameters for full molecules to parameterize beads representing fragments.

IV. CONCLUSION

This study examined the automatic parameterization of DPD using activity coefficients derived from COSMO-SAC predictions in quantitative detail. Three issues with parameterization were highlighted: the inability of individual beads to reproduce infinite dilution activity coefficients generated by COSMO-SAC, the errors involved with reusing beads for identically structured fragments in different molecules, and the effects of bonding beads together. Of the three issues listed, the first is of greatest consequence and can result in grossly inaccurate results—especially when water is being simulated. This issue should be addressed in future studies, especially when water makes up one of multiple phases in a simulation. In addition, the coarse graining of multiple water molecules into a single DPD bead induces small but significant errors in the partitioning behavior with respect to the experiment.

The strategy that was presented for correcting some of the bonding effects significantly improved the partition coefficient calculations—bringing the maximum deviation of the logarithm partition coefficient to within 0.40. This method is not perfect, and further improvements can be made. For example, it can be extended to a larger range of repulsion parameters, or it could be altered to correct for the bonded solute effect while not negatively affecting the bonded solvent effect. However, the method as it is presented here demonstrates that COSMO-SAC parameters can be mapped onto DPD to a high level of precision.

SUPPLEMENTARY MATERIAL

See supplementary material for additional data.

ACKNOWLEDGMENTS

The author would like to acknowledge Dr. Jan-Willem Handgraaf from Culgi BV for his instruction on how to use the CULGI modeling platform and Dr. Michael Harper from ExxonMobil Research and Engineering Company for his helpful input on this paper.

[1]P. J. Hoogerbrugge and J. M. V. A. Koelman, Europhys. Lett. **19**, 155 (1992).
[2]P. Español and P. Warren, Europhys. Lett. **30**, 191 (1995).
[3]R. D. Groot and P. B. Warren, J. Chem. Phys. **107**, 4423 (1997).
[4]C. M. Wijmans, B. Smit, and R. D. Groot, J. Chem. Phys. **114**, 7644 (2001).
[5]R. D. Groot, Langmuir **16**, 7493 (2000).
[6]J. Cheng, A. Vishnyakov, and A. V. Neimark, Langmuir **30**, 12932 (2014).
[7]G. Pan and C. W. Manke, J. Rheol. **46**, 1221 (2002).
[8]P. Padmanabhan, F. Martinez-Veracoechea, and F. A. Escobedo, Macromolecules **49**, 5232 (2016).
[9]R. D. Groot and T. J. Madden, J. Chem. Phys. **108**, 8713 (1998).
[10]R. D. Groot, T. J. Madden, and D. J. Tildesley, J. Chem. Phys. **110**, 9739 (1999).
[11]X. Cao, G. Xu, Y. Li, and Z. Zhang, J. Phys. Chem. A **109**, 10418 (2005).
[12]S. Yamamoto, Y. Maruyama, and S.-A. Hyodo, J. Chem. Phys. **116**, 5842 (2002).
[13]J. C. Shillcock and R. Lipowsky, J. Chem. Phys. **117**, 5048 (2002).
[14]V. Ortiz, S. O. Nielsen, D. E. Discher, M. L. Klein, R. Lipowsky, and J. Shillcock, J. Phys. Chem. B **109**, 17708 (2005).
[15]L. Gao, J. Shillcock, and R. Lipowsky, J. Chem. Phys. **126**, 015101 (2007).
[16]R. D. Groot and K. L. Rabone, Biophys. J. **81**, 725 (2001).
[17]L. Rekvig, M. Kranenburg, J. Vreede, B. Hafskjold, and B. Smit, Langmuir **19**, 8195 (2003).
[18]E. Mayoral and A. G. Goicochea, J. Chem. Phys. **138**, 094703 (2013).
[19]A. Vishnyakov, M.-T. Lee, and A. V. Neimark, J. Phys. Chem. Lett. **4**, 797 (2013).
[20]M.-T. Lee, A. Vishnyakov, and A. V. Neimark, J. Phys. Chem. B **117**, 10304 (2013).
[21]J. G. E. M. Fraaije, K. Tandon, S. Jain, J.-W. Handgraaf, and M. Buijse, Langmuir **29**, 2136 (2013).
[22]Y. Ruiz-Morales and O. C. Mullins, Energy Fuels **29**, 1597 (2015).
[23]M.-T. Lee, R. Mao, A. Vishnyakov, and A. V. Neimark, J. Phys. Chem. B **120**, 4980 (2016).
[24]S.-F. Zhang, L.-L. Sun, J.-B. Xu, H. Wu, and H. Wen, Energy Fuels **24**, 4312 (2010).
[25]J. G. E. M. Fraaije, J. van Male, P. Becherer, and R. Serral Graciá, J. Chem. Inf. Model. **56**, 2361 (2016).
[26]R. L. Anderson, D. J. Bray, A. S. Ferrante, M. G. Noro, I. P. Stott, and P. B. Warren, J. Chem. Phys. **147**, 094503 (2017).
[27]T. P. Liyana-Arachchi, S. N. Jamadagni, D. Eike, P. H. Koenig, and J. I. Siepmann, J. Chem. Phys. **142**, 044902 (2015).
[28]B. V. Culgi, The Chemistry Unified Language Interface (Culgi), version 10, The Netherlands (2004-2016).

[29]A. Klamt, J. Phys. Chem. **99**, 2224 (1995).
[30]S.-T. Lin and S. I. Sandler, Ind. Eng. Chem. Res. **41**, 899 (2002).
[31]H. Alasiri and W. G. Chapman, J. Mol. Liq. **246**, 131 (2017).
[32]A. J. Staverman, Recl. Trav. Chim. Pays-Bas **69**, 163 (1950).
[33]E. A. Guggenheim, *Mixtures: The Theory of the Equilibrium Properties of Some Simple Classes of Mixtures Solutions and Alloys* (Clarendon Press, 1952).
[34]S. Plimpton, J. Comput. Phys. **117**, 1 (1995).
[35]P. C. Hiemenz and T. P. Lodge, *Polymer Chemistry* (CRC Press, 2007).
[36]B. A. van der Rotten, "A limited memory Broyden method to solve high-dimensional systems of nonlinear equations," Ph.D. thesis, Mathematisch Instituut, Universiteit Leiden, 2003.
[37]S.-T. Lin and S. I. Sandler, Ind. Eng. Chem. Res. **38**, 4081 (1999).